A major purpose of the Technical Information Center is to provide the broadest dissemination possible of information contained in DOE's Research and Development Reports to business, industry, the academic community, and federal, state and local governments.

Although portions of this report are not reproducible, it is being made available in microfiche to facilitate the availability of those parts of the document which are legible.

DF 7.1448-6

Los Alamos National Laboratory is operated by the University of California for the United States Department of Energy under contract W-7405-ENG-36

CONF-8405164--1

TITLE: SOLA-LOOP ANALYSIS OF A BACK PRESSURE CHECK VALVE

AUTHOR(S): J. R. Travis

LA-UR--84-1620

DE84 012437

SUBMITTED TO: IAEA Technical Committee/Workshop on the Uses of Computer Codes for Nuclear Reactor Safety Analysis, Varna, Bulgaria, 28 May - 1 June 1984.

DISCLAIMER

MASTER

Los Alamos Los Alamos National Laboratory
Los Alamos, New Mexico 87545

SOLA-LOOP ANALYSIS OF A BACK-PRESSURE CHECK VALVE

J. R. Travis

Theoretical Division, Group T-3
University of California
Los Alamos National Laboratory
Los Alamos, New Mexico 87545

ABSTRACT

The SOLA-LOOP computer code for transient, nonequilibrium, two-phase flows in networks has been coupled with a simple valve model to analysis a feed-water pipe breakage with a back-pressure check valve. Three tests from the Superheated Steam Reactor Safety Program Project (PHDR) at Kahl, West Germany are analyzed, and the calculated transient back-pressure check valve behavior and fluid dynamics effects are found to be in excellent agreement with the experimentally measured data.

I. INTRODUCTION

Should a feed-water pipe in a nuclear power plant break, the feed-water back-pressure check valve has the function of limiting the loss of coolant. The check valve must close quickly, with the result that the escaping fluid comes to rest in a very short period of time. Forces are developed in the pipe by the rapid closure of the valve that may lead to stresses of considerable magnitude on the valve, pipe and supports. The so-called "fast-slow" feed-water back-pressure check valves have been designed to solve this problem. These valves have an optimized damping mechanism so that the last part of the closure stroke is very slow, thus minimizing the water-hammer effects.

An experimental performance analysis has been conducted [1] by the PHDR of the Kernforschungszentrum in Karlsruhe utilizing a full scale previously operational single loop pressurized water reactor facility. The German blowdown experiments, with which we are to compare the SOLA-LOOP calculated results, consisted of three tests. It was the objective of these tests to investigate the closure of the feed-water back-pressure check valve and the fluid dynamics in the piping network following a sudden pipe rupture.

II. EXPERIMENTAL FACILITY

The pipe system used for the blowdown experiments, including the auxiliary devices, is shown in Fig. 1. The steady state flow path leads from the S-connector (3) of the reactor pressure vessel (1) through a ball-shaped fitting (13), the suction-side shut-off gate valve (6), the circulation pump (7), the quick-action stop valve (5), the T-fitting (12), the measuring ring II (10), the experimental check valve (4), and measuring ring I (9) back to the reactor pressure tank (1). On the other side of the T-filling (12), the rupture connector (3) connects with the rupture disk device and the measuring ring III (11).

At the initialization of the flow conditions, the circulation pump establishes a flow rate of approximately 1600 m^3/h, which corresponds to a average steady state flow velocity of roughly 4.0 m/s in the pipe loop. At the moment the rupture disks break, the circulation pump (7) is shut off, and the quick-action stop valve (5) has the function of closing off the S-loop in about 1 s. As a further shut-off device in the S-loop, there is also a shut-off gate valve (6) which takes about 2 min to close.

To initiate the blowdown, the pressure between the two rupture disks is raised quickly so that the outer disk is blown out the end of the pipe. This results in a large pressure differential across the inner rupture disk and it is also blown out. The pipe cross-section is completely opened within 3 ms.

The experimental valve is a feed-water back-pressure check valve with hydraulic end damping. Figure 2 shows the check valve in the horizontal plane of the pipe axis as it is installed in the experimental superheated steam reactor plant. The valve apparatus is installed in the housing at an angle of 45 degrees, with the movable valve head (K) and the damping piston (D) both rigidly connected to the spindle (S).

Upon blowdown, the normal flow shown in Fig. 2 from left to right is reversed and the valve head moves from the open position shown to the closed position with the valve head seating in the valve throat. This motion is at first fast but in its final phase much slower as damping begins as soon as the annular gap between the cylinder and the damping piston narrows to a small width as the damping piston lowers. Figure 3 shows the damping design with the gentle taper between the larger cylindrical diameter (very little damping) to the smaller cylindrical diameter (maximum damping). The valve head closing rate depends on the resistance the annular gap presents to the flow of water from the chamber under the piston. For experiments V60.1 and V60.2 the annular gap is 0.3 mm, and experiment V60.3 has an annular gap equal to 1.3 mm. Less flow resistance, for example, can be designed into the damping phase by increasing the annular gap width or by decreasing the roughness of the annular surfaces.

III. DESCRIPTION OF THE THEORETICAL MODEL

The SOLA-LOOP [2] computer code has been utilized to calculate the flow in the pipe network shown in Fig. 1. SOLA-LOOP is a sophisticated yet fairly simple, very user friendly, highly flexible computer code for transient, nonequilibrium, two-phase flow in networks. Each component may have a one-dimensional representation with variable cross-sectional area. The flow dynamics is governed by a set of nonlinear conservation laws based on a generalized drift-flux model for two-phase mixtures. The equations are solved by a partially implicit finite-

difference method (ICE: Implicit Continuous-fluid Eulerian [3]) that can use different time steps in different components. The complete equations and constitutive relations describing interphase transfers of mass, momentum, and energy, as well as the details of the numerical solution technique can be found in Ref. 2. For the purposes of this paper, only a brief sketch of a reduced form of these equations is given here.

At the flow rates of interest, it is anticipated that the relative velocity between phases will be small. Therefore, for this discussion we assume that the two phases comprising the fluid mixture move with the same average velocity.

In the case of equal phase velocities (mechanical equilibrium) and equal phase temperatures (thermal equilibrium), the governing equations for the two phase mixture density, ρ, velocity, u, and internal energy, I, reduce to

$$\frac{\partial \rho}{\partial t} + \frac{1}{A}\frac{\partial}{\partial y}(A\rho u) = 0 \quad , \tag{1}$$

$$\frac{\partial \rho u}{\partial t} + \frac{1}{A}\frac{\partial}{\partial y}(A\rho u^2) = -\frac{\partial P}{\partial y} + f_{vis} \quad , \tag{2}$$

$$\frac{\partial \rho I}{\partial t} + \frac{1}{A}\frac{\partial}{\partial y}(A\rho I u) = -\frac{P}{A}\frac{\partial}{\partial y}(Au) + W_{vis} \quad , \tag{3}$$

where A is the time-independent, cross-sectional area of the flow channel or pipe. Local flow losses from rapid area changes are accounted for by adding the necessary pressure loss and energy dissipation to Eqs. (2) and (3) through the terms f_{vis} and W_{vis}, respectively. In addition, the term f_{vis} accounts for pressure losses due to pipe wall friction. These equations must be supplemented with an equation for the macroscopic vapor density, ρ_v,

$$\frac{\partial \rho_v}{\partial t} + \frac{1}{A}\frac{\partial}{\partial y}(A\rho_v u) = \Gamma \quad , \tag{4}$$

where Γ is the rate of production of vapor mass per unit volume and time. For the present study, we have assumed that the vapor and liquid temperatures are both equal to the saturation temperature (thermal equilibrium). This is accomplished by choosing a vapor production rate of the form

$$\Gamma = C(T_\ell - T_s) \quad , \tag{5}$$

where T_ℓ and T_s are the liquid and saturation temperatures, respectively. The coefficient, C, is set sufficiently large to insure a large vapor production rate to produce nearly continuous equilibrium states in which the liquid, gas, and saturation temperatures are the same. This development leads to what is commonly called the homogeneous equilibrium model (HEM).

In order to include the dynamical effect of the back-pressure check valve on the fluid dynamics, it is necessary to couple a valve model to SOLA-LOOP. This coupling is accomplished with SOLA-LOOP supplying time-dependent fluid velocities, densities, and pressures to the valve model, and in return, the valve model calculates a time-dependent valve head position (stroke), which is used to determine the resistance to flow through the valve.

The equilibrium of forces on the valve head is established by the acceleration, the pressure force of the fluid, the damping force of the valve, the gravitational force, as well as any external actuating force and/or spring support of the movement of the valve. This force balance for the valve model is given by

$$m\frac{d^2x}{dt^2} = \sum F \quad ,$$

where the forces are: (1) pressure force, (2) hydraulic damping force, (3) external actuating force, and (4) gravitational force.

The dynamical behavior of the check valve influences the fluid dynamics through a pressure loss in the f_{vis} term in Eq. (2). This pressure loss is represented, $\Delta p = \xi_v(\frac{1}{2}\rho V^2)$, where ρ and V are the upstream fluid density and velocity, respectively, and ξ_v is the valve position dependent flow loss coefficient. There are two ways of accounting for this pressure loss. The first is to sum the effects of actually changing the area open to flow in

the mesh cell represented the value and adding a pressure loss such that the total loss from the time dependent area change plus the added pressure loss equals the desired total pressure loss. The second method is to derive the same pressure loss by ignoring the area change and simply modeling a functional pressure loss. We have elected to make use of the second of these methods because the numerical loss associated with physically changing the area is not well known, and for the second method, it is simply a matter of being consistant in choosing the flow loss coefficient and velocity position. Reference 4 lists steady state values for this resistance coefficient as a function of the valve position or stroke. We have found in comparisons with data from the three experiments discussed in the next section that these steady state resistances are less than what are actually needed. It has been shown [5] that with decelerating flows, the resistance is appreciably more than for the equivalent steady state. This is consistent with our findings, and therefore, has lead us to develop our own position dependent flow loss coefficient based upon the unsteady transient experiments discussed in the next section.

IV. EXPERIMENTAL AND COMPUTATIONAL RESULTS

The test parameters for the three tests are as follows:

V60.1 - Test with normal BWR - design conditions and with near optimized damping in the check valve.

V60.2 - Test with the same check valve damping as in V60.1 but with stronger thermodynamic conditions due to the cold water in the test pipe.

V60.3 - Test with normal BWR - design conditions but with reduced damping in the check valve.

The boundary and initial conditions are:

length of the test pipe	:	15.0 m
diameter of the test pipe	:	371.4 mm
diameter of the rupture nozzle	:	453.0 mm
pressure in the vessel	:	70.0 bar
temperature in the vessel	:	285.0°C
temperature in the pipe		
V60.1 and V60.3	:	220.0°C
V60.2	:	50.0°C
valve position	:	98.0 mm
velocity in pipe	:	4.0 m/s

In Figs. 4, 5, and 6, the time history of the valve position, there is an undamped run from the initial position to roughly 75 mm. At that time (approximately 0.03 s) the annular gap has decreased so that hydraulic damping becomes important. This is evidenced by the dramatic change in the slope of the closing curves, at least in tests V60.1 and V60.2, in an attempt to soften or minimize the water-hammer effect. In test V60.3 the closure rate is largely unaffected by damping, although it is noted that there is a slight slope change at 75 mm or 0.03 s as well. As the valve continues to close, there is another change in the closing curve slope for V60.1 and V60.2 at approximately 55 mm (0.15 s) or just before the curves become linear. For V60.3 the linear portion of the closing curve does not start until the valve has closed to about 45 mm or roughly 0.1 s. Reference 1 lists the closing times of 605 ms, 594 ms, and 145 ms for V60.1, V60.2, and V60.3, respectively. In these comparisons and the ones to follow, the calculated curves are designated with triangles while the measured experimental data are shown unmarked.

Pressure histories just upstream of the value for the three experiments and calculations are presented in Figs. 7, 8, and 9. The rather sharp pressure spike at 0.03 s for all three experiments is a result of the change in the closing curve slope at that time. Additionally, there are local pressure maxima corresponding in time to the other closing curve slopes changes, namely 0.15 s for V60.1 (Fig. 7) and V60.2 (Fig. 8) and 0.1 s for V60.3 (Fig. 9). Through the linear portion of the closing curve until the valve is actually closed, there is relatively very little pressure change; however, after closing, the water-hammer effect is dramatically shown in all three experiments. For tests V60.1 (Fig. 7) and V60.2 (Fig. 8), this water-hammer is in the neighborhood of 10 - 13 bars, while in V60.3, where the closure rate is largely unaffected by hydraulic damping, and consequently, the water-hammer is very pronounce and closer to 70 bars. The water-hammer or 1/4 period pressure waves are set up in the isolated pipe between the closed valve and the pressure vessel. These waves are shown to decay in time. Pressure histories on the downstream side of the valve are presented in Figs. 10, 11, and 12. After the initial transient of roughly 0.1 s, the first closing curve change of slope is reflected in the sharp spike at 0.03 s, the pressures quickly approach their saturated values corresponding to the liquid temperature. Mass flow rate measurements at measuring ring I (Figs. 13, 14, and 15) exhibit an initial fluid acceleration through the valve (times < 0.1 s) and then deceleration as the flow resistance increases corresponding to the valve closing.

Recall that the difference between experiments V60.1 and V60.2 is that in V60.2 the fluid temperature is 50°C as opposed to 220°C temperature in V60.1. The main distinction between these, otherwise identical, experiments shows up in the downstream pressure histories (Figs. 10 and 11) and the mass flow rates (Figs. 13 and 14).

After the initial transient, the pressure for V60.1 is about 2.3×10^6 Pa (23 bar) as contrasted to roughly 1.2×10^4 Pa (0.12 bar) for V60.2. These pressures correspond to saturation pressure for the fluid temperature, respectively. With flashing occurring in the valve throat, the mass flow rate reaches critical values which are

dependent upon the pressure through the valve. Consequently, the maximum mass flow rate for V60.2 is approximately 35% greater than V60.1. Notice that V60.1 and V60.3 exhibit some leakage past the valve after it is supposedly closed. This is evidenced by the positive mass flow rates after valve closing. In fact for V60.3 (Fig. 15), it appears from the experimental data that the valve head actually rebounds at approximately 0.5 s.

V. MODING AND ACCURACY CONSIDERATIONS

In any numerical integration method, it is important to assess the accuracy of the approximations. In the present case, this is done in two ways. The first and most straightforward method is to increase the resolution of the finite difference mesh. This is also, computationally, the most costly method. In the SOLA-LOOP code, there is a second, more efficient method to check errors induced by numerical diffusion. All convective flux terms in the SOLA-LOOP code are approximated by a mixture of centered and upstream or donor cell finite difference expressions. The mixture is controlled by an input parameter ALPHA, such that a value of unity for ALPHA results in donor cell differencing, while a zero value corresponds to centered differencing. For numerical stability, it is generally necessary that ALPHA remain greater than the largest value of $|u|\delta t/\delta y$ occurring in the mesh. However, the closer ALPHA is to this stability limit, the smaller will be the numerical diffusion. Both of these accuracy checks have been incorporated in developing confidence in the numerical solution. The final mesh configuration was determined after applying mesh refinements and setting ALPHA close to the stability limit with the resulting effect being only small changes in the solution.

VI. CONCLUSIONS

It has been demonstrated that the coupling of numerical tools, such as SOLA-LOOP and a model for the dynamic behavior of a back-pressure check valve, can be a tremendous help in designing complex network system components in order to achieve near optimum performance characteristics. Calculated results are seen to be in excellent agreement with the overall experimental data and in remarkably good agreement with the fine structure and features of the measured quantities.

ACKNOWLEDGEMENTS

The author wishes to express his appreciation for discussions with F. H. Harlow and M. D. Torrey. This work was supported by the United States Nuclear Regulatory Commission, Division of Reactor Safety Research, Washington, DC.

REFERENCES

1. "Investigations of Feed-Water Back-Pressure Valve NW350 upon Breakage of a Reactor Coolant Medium Pipe, Quick Look Report, SRV350," Techn. Fachbericht PHDR 11-80 (April 1980).

2. C. W. Hirt, T. A. Oliphant, W. C. Rivard, N. C. Romero, and M. D. Torrey, "SOLA-LOOP: A Nonequilibrium, Drift-Flux Code for Two-Phase Flow in Networks," Los Alamos National Laboratory report LA-7659 (June 1979).

3. F. H. Harlow and A. A. Amsden, "A Numerical Fluid Dynamics Calculation Method for All Flow Speeds," J. Comput. Phys. 8, 197 (1971).

4. T. Grillenberger, "German Standard Problem No. 4: Breakage of a Feed-Water Pipe with a Back-Pressure Valve, Specification," June 1980.

5. J. W. Daily, W. L. Hankey, Jr., R. W. Olive, and J. M. Jordaan, Jr., "Resistance Coefficients for Accelerated and Decelerated Flows Through Smooth Tubes and Orifices," Trans. ASME, 78, No. 5, pp. 1071 (July 1956).

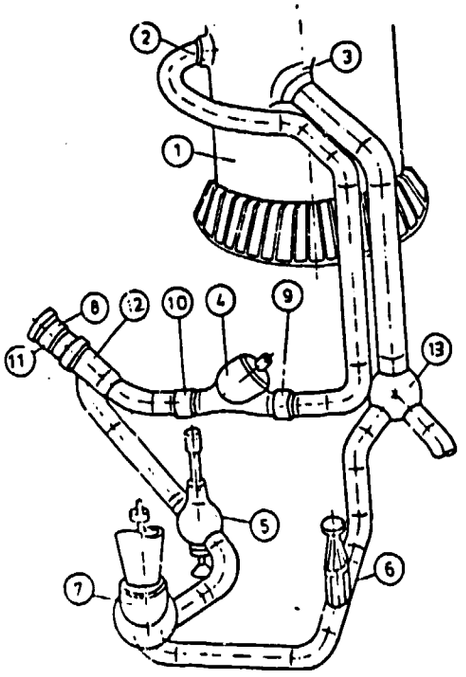

1 Reactor pressure tank (RPT)
2 T-connector
3 S-connector
4 Experimental valve
5 Quick-action stop valve
6 Shut-off gate valve
7 Circulation pump
8 Rupture connector
9 Measuring ring I
10 Measuring ring II
11 Measuring ring III
12 T-fitting
13 Ball fitting

Fig. 1. Experimental pipe system (from Ref. 1).

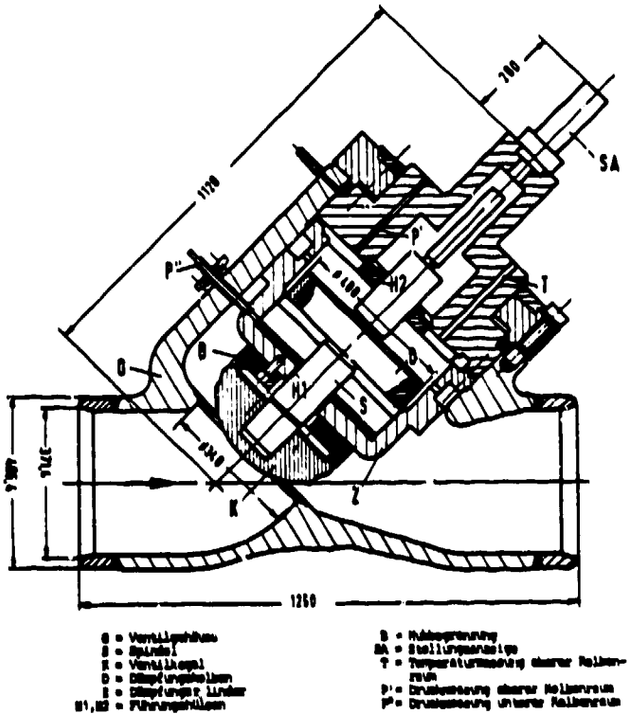

Fig. 2. Back-Pressure Check Valve (from Ref. 1).

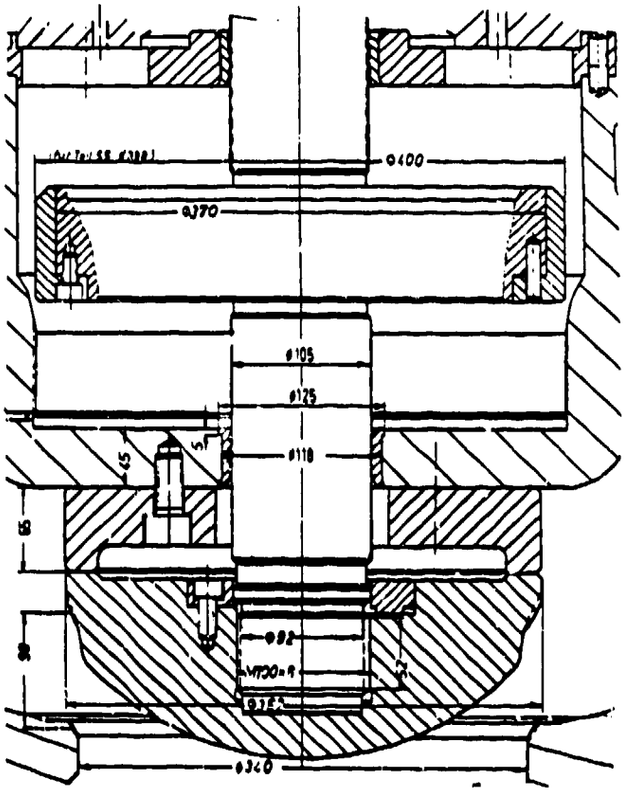

Fig. 3. Valve head, damping-piston, and damping chamber (from Ref. 1).

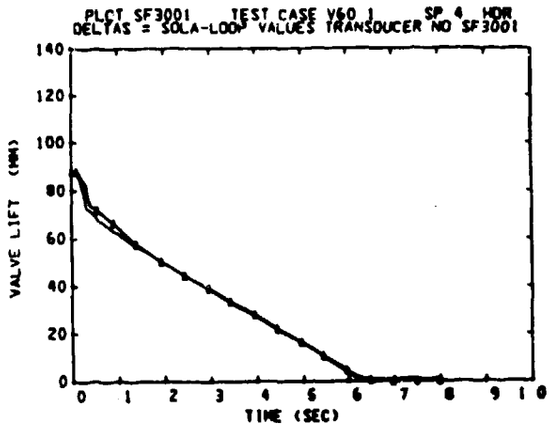

Fig. 6. Valve piston for V60.1 (calculated results are shown as triangles).

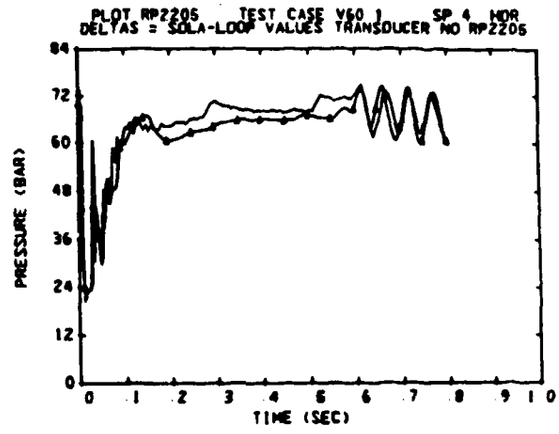

Fig. 7. Pressure upstream of valve for V60.1 (calculated results are shown as triangles).

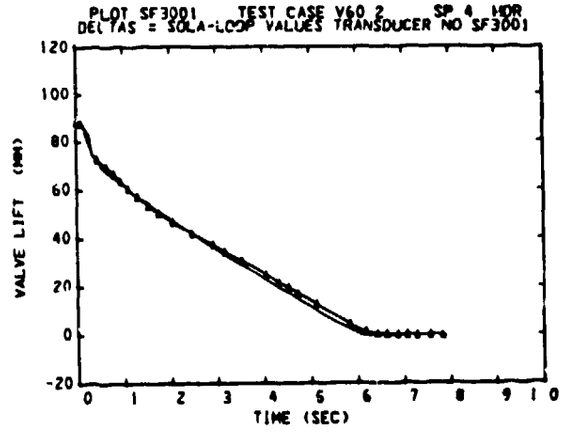

Fig. 8. Valve position for V60.2 (calculated results are shown as triangles).

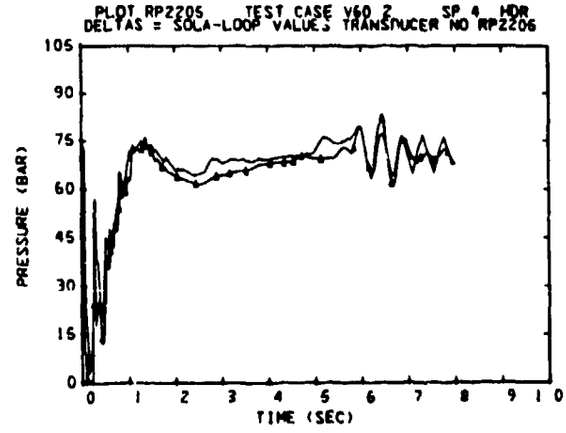

Fig. 9. Pressure upstream of valve for V60.2 (calculated results are shown as triangles).

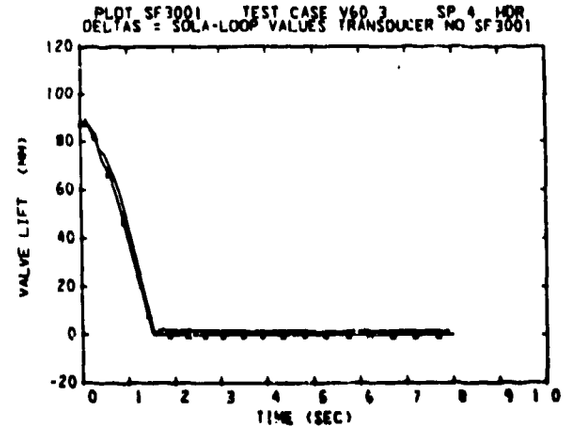

Fig. 10. Valve position for V60.3 (calculated results are shown as triangles).

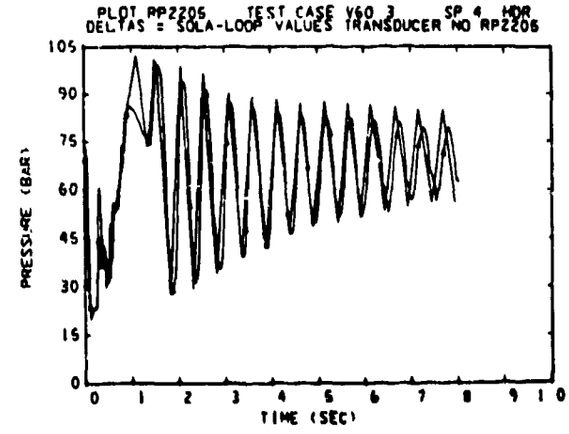

Fig. 11. Pressure upstream of valve for V60.3 (calculated results are shown as triangles).

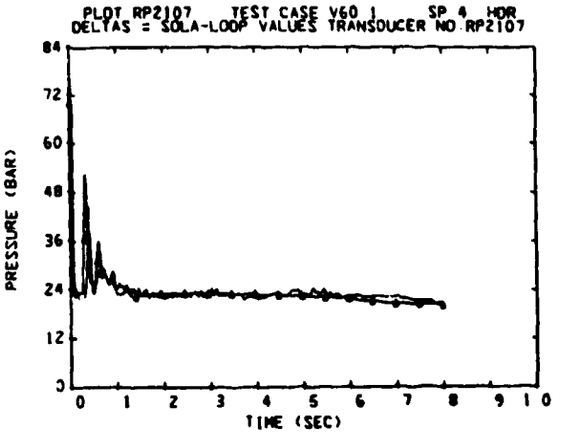

Fig. 10. Pressure downstream of valve for V60.1
(calculated results are shown as triangles).

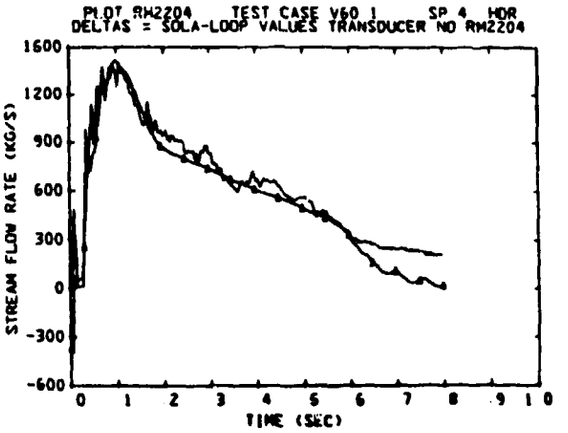

Fig. 13. Mass flow rate of measuring ring I for V60.1
(calculated results are shown as triangles).

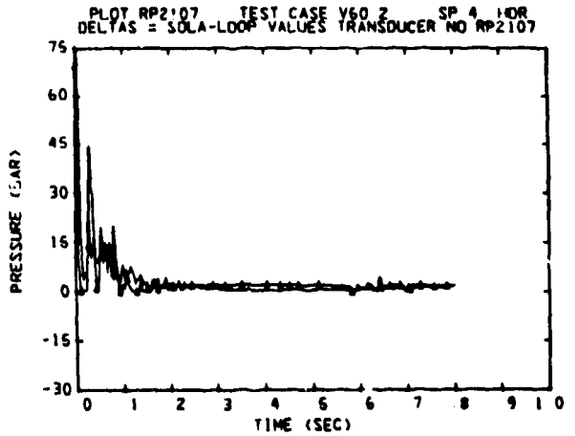

Fig. 11. Pressure downstream of valve for V60.2
(calculated results are shown as triangles).

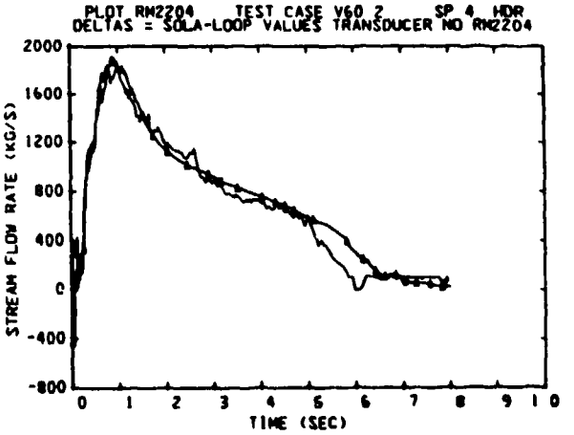

Fig. 14. Mass flow rate at measuring ring I for V60.2
(calculated results are shown as triangles).

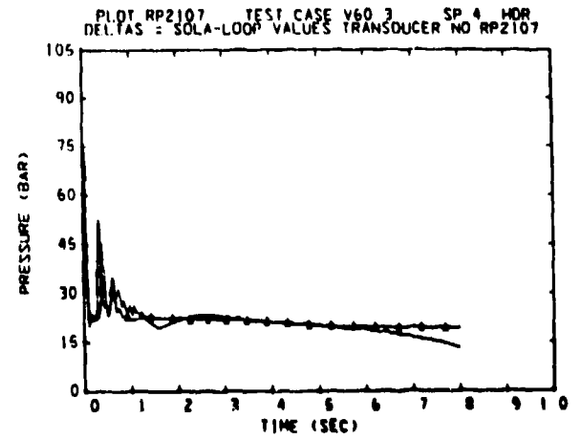

Fig. 12. Pressure downstream of valve for V60.3
(calculated results are shown as triangles).

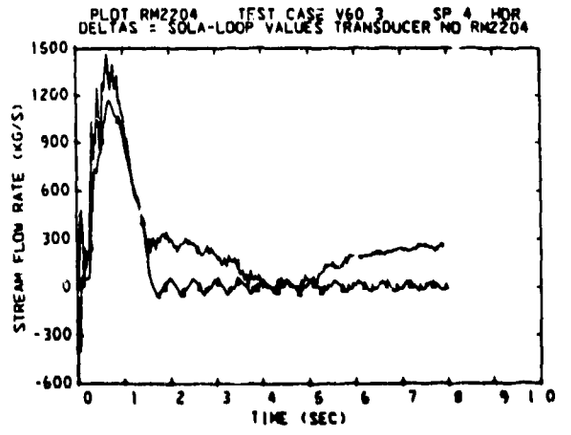

Fig. 15. Mass flow rate of measuring ring I for V60.3
(calculated results are shown as triangles).